Robust Design of a TCSC Oscillation Damping Controller in a Weak 500-kV Interconnection Considering Multiple Power Flow Scenarios and External Disturbances

Alberto M. Simões, Diego C. Savelli, Paulo C. Pellanda, *Member, IEEE*, Nelson Martins, *Fellow, IEEE*, and Pierre Apkarian, *Member, IEEE*

***Abstract*— The Power Oscillation Damping (POD) controllers implemented in the two thyristor controlled series compensators of the Brazilian North-South (NS) interconnection, in the year 1999, were solely intended to damp the low-frequency NS oscillation mode. These controllers are still under operation and are derived from the modulus of the active power flow in the NS line that is phase-lagged at the frequency of the NS mode and may experience relatively large excursions generated by exogenous disturbances. This paper utilizes the same 1999 data to compare the performance of a proposed robust POD controller design with those of two conventional designs. A recent robust control synthesis algorithm here utilized is based on a nonsmooth optimization technique and has the capability to handle various controller structures, including reduced-order, and to deal with time-domain constraints on both controlled and measured outputs. Moreover, the nonsmooth design technique encompasses multiple operating conditions subject to various test signals hence building a truly time-domain multi-scenarios approach. According to the results discussed hereafter this is a key advantage in the industrial context of increasing demand for performance and robustness. The described results relate to a large-scale system model used in the feasibility studies for that interconnection.**

***Index Terms*— Small-Signal Stability, Large Scale Systems, FACTS, Electromechanical Oscillations, Robust Control, Control Design, Disturbance Rejection, Modal Analysis, Frequency Response, Time-Domain Constraints, Nonsmooth Optimization.**

I. Introduction

THE interconnection of the North-Northeast and the South-Southeast Brazilian subsystems (called North and South subsystems in this paper) in 1999, caused the emergence of a new poorly-damped, low-frequency ($0.17 - 0.25$ Hz) swing mode: the North-South (NS) mode [1]–[4]. Thyristor Controlled Series Compensators (TCSCs) [5]–[8] equipped with Power Oscillation Damping (POD) controllers were installed at the North and South ends of the NS intertie, with the sole objetive of damping the NS mode. A cost-effective POD design should yield not only good oscillation damping but also moderate transients in the POD output signal, following exogenous disturbances. Due to the finite equipment ratings, a large POD output signal may cause the TCSC to hit its limits. If the TCSC hits limits at every half cycle of the NS mode, the effective magnitude and phase compensation will differ from the intended values, drastically reducing the POD damping control action. Checking equipment performance for exogenous disturbances, such as generating-unit rejections and the ensuing active power surges, is therefore an integral part of POD controller design.

The single machine-infinite bus example in Fig. 1 is used to demonstrate the impact of TCSC limits in reducing the intended damping of the critical mode. This example relates to a 1,275 MVA power plant supplying 560 MW through a 500 km long transmission line whose parameters are identical to those of the NS intertie. The generator is equipped with fast exciter but no PSS. The electromechanical oscillation damping control is exerted by a POD-equipped TCSC in this line. A single-phase to ground fault is applied to the transmission line for 100 ms, and then removed without line opening. The ensuing transients are simulated considering three different MVAr capacities for the TCSC. It is clear from the nonlinear simulated results that a reduction in the TCSC MVAr capacity causes it to hit limits more severely and for a longer period with detrimental impact to its damping control capability.

Publications from several sources focused on the stabilization of the NS mode either through retuning of the existing Power System Stabilizers (PSSs) at the three major Northeast power plants [1], [9] or installation of TCSCs equipped with PODs at the two ends of the NS line [1]–[4], [9], [10]. These two damping control options are currently implemented in the actual system, providing a comfortable level of redundancy of damping sources, but this paper focuses only on the TCSC solution. Previous valuable work on POD modulated by TCSCs is vast, including [11]–[15].

The TCSC at the North end (Imperatriz substation, IZ) was supplied by ABB while the other at the South end (Serra da

Manuscript received

Alberto M. Simões is with ONERA-CERT-Control System Department, 2 av. Edouard Belin, 31055 Toulouse, France (alberto.simoes@cert.fr), and is supported by the Brazilian Army.

Diego C. Savelli is with TRANSPETRO, Av. Presidente Vargas, 328, Rio de Janeiro, RJ - 20091-060, Brazil (diegosavelli@petrobras.com.br).

Paulo C. Pellanda is with IME-Instituto Militar de Engenharia, Praça General Tibúrcio, 80, Praia Vermelha, Rio de Janeiro, RJ - 22290-270, Brazil (pcpellanda@ieee.org, pellanda@ime.eb.br).

Nelson Martins is with CEPEL, P.O.Box 68007, Rio de Janeiro, RJ - 20001-970, Brazil (nelson@cepel.br).

Pierre Apkarian is with ONERA-CERT-Control System Department and Université Paul Sabatier, Institut de Mathématiques, Toulouse, France (apkarian@cert.fr).

Digital Object Identifier XX.XXXX/TPWRS.XXXX.XXXXXX.

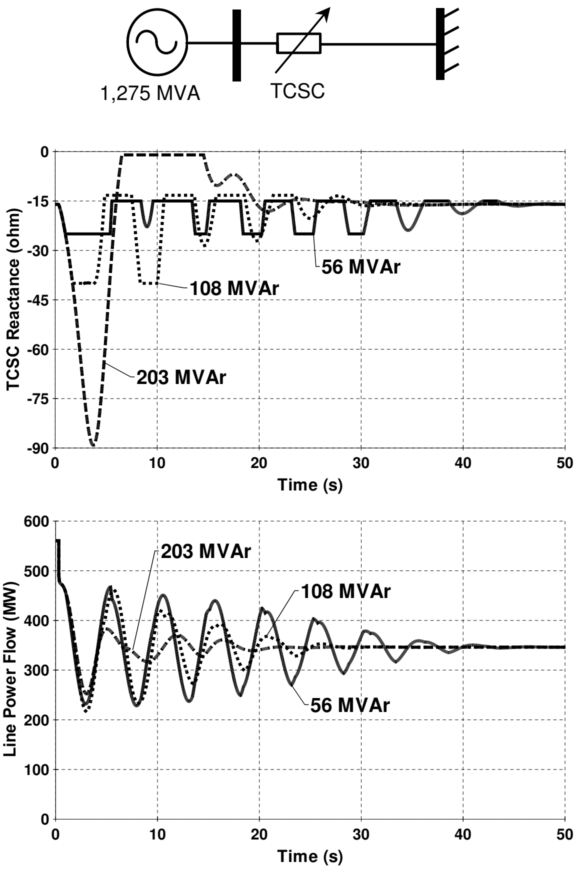

Fig. 1. Impact of TCSC limits on the power flow oscillation damping of a single machine-infinite bus example.

Mesa substation, SMA) was supplied by Siemens, their PODs being designed according to distinct control philosophies [3], [4]. This paper utilizes the SMA POD for the studies of the proposed POD signal, since it presents slightly greater challenges in its design due to the close proximity of the SMA power station. The existing POD at the Imperatriz substation (IZ POD) is based on an innovative concept that ensures good performance under exogenous disturbances, requiring, however, the online estimation of the frequency to be damped. The IZ POD requires more complex modeling for the correct assessment of its dynamic performance, under a linear analysis perspective, and will be the object of a future publication. The IZ POD was considered to be disconnected in the studies since this does not impact the focus of this paper.

The objectives of the paper are the following:

- test the effectiveness of a recent nonsmooth design technique [16], [17] in a realistic multi-scenarios large system;
- synthesis of robust POD controllers to stabilize the inter-area mode without destabilizing other modes, considering multiple power flow scenarios;
- analysis of adverse transients that lead the POD-equipped TCSC to hit its limits, following exogenous disturbances, comparing the performance of the robust POD design against those of conventional designs.

This paper is of an exploratory nature and does not reflect the viewpoints of the manufacturers, Brazilian utilities or system operator. Also, the Brazilian Interconnected Power System (BIPS) has greatly evolved since 1999, currently existing three circuits interconnecting the NS regions, besides a Southeast-Northeast interconnection whose combined effect has raised the NS mode frequency to over 0.3 Hz and eliminated the originally critical damping problem.

The apparent simplicity of the POD design objectives (single mode damping) is actually very deceptive, since a series of issues impose very challenging design constraints: different levels of power transfer and system configuration, power flow reversal, level of POD induced adverse transients that lead the TCSC to hit limits, adverse interactions among nearby high-performance controllers, etc.

This paper is organized as follows. Section II describes the problem of adverse transients in the POD control loop. The Modal Dominance Index (MDI) used for the computation of reduced equivalents is defined in Section III. Section IV proposes a robust control synthesis based on a nonsmooth optimization technique for solving the POD controller design problem. Conventional POD controllers are discussed in Section V while Section VI describes the results that support the proposed robust POD synthesis. Section VII concludes.

II. Control and Disturbance Models

The test system data correspond to a year 1999 planning model, having 2,370 buses, 3,401 lines, 123 synchronous machines plus field excitation and speed-governor controls, 46 power system stabilizers, 4 static var compensators, two TCSCs equipped with POD controllers (one of which is the object of design in this paper), and one large HVDC link. Each generator and associated controls, with a few exceptions, is the aggregate model of a whole power plant. The schematic diagram of BIPS, highlighting the SMA TCSC, is shown in Fig. 2. The seventeen base case scenarios, utilized in one of the several planning studies of the NS interconnection [18], were considered to ensure controller robustness. All control analysis and conventional design studies were carried out using the large BIPS model rather than reduced equivalents. Reduced equivalents with 200 states were used only for the design of the robust nonsmooth time domain controller [16], [17], but the performance verification tests used the large model. Modal equivalencing [19], [20] was used because the high system order precluded the use of other well proven techniques, such as Balanced Truncation [15], [21].

The scenario in which the NS mode is the least-damped (scenario I in Table I) was used as the reference scenario. This scenario has a total load of 46,000 MW, with the North exporting 1,000 MW to the South, through the planned 500 kV, 1,000 Km long, series compensated NS intertie. The state space realization of the BIPS model has 1,664 states and the sparse, unreduced Jacobian has dimension 13,251. The sparse Jacobian structure and the full eigenvalue spectrum, for this 1,664-state BIPS model, are pictured in [22]. This model correctly reproduces the low-frequency and poor-damping characteristics of the NS mode.

The BIPS variable from which the POD feedback is derived is the module of the active power in the NS line. This signal

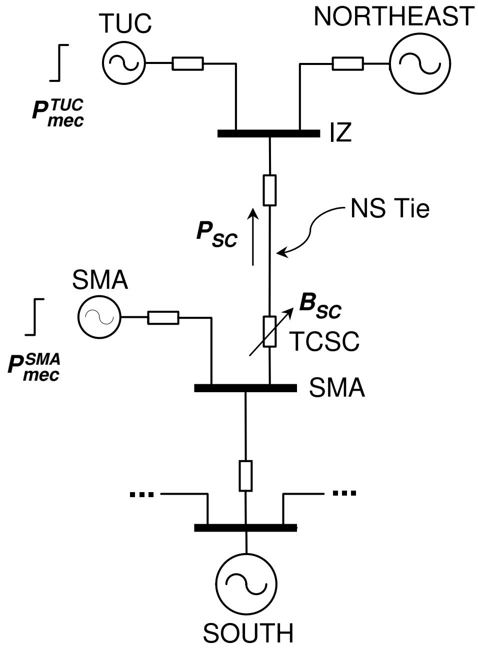

Fig. 2. Schematic diagram of Brazilian Interconnected Power System (BIPS) in year 1999. Acronyms SMA, TUC, IZ denote Serra da Mesa, Tucuruí and Imperatriz power plants or substations.

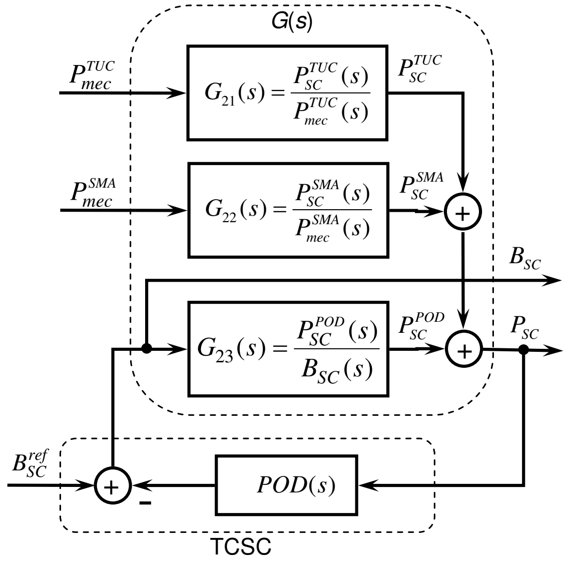

Fig. 3. BIPS model used for robust POD controller analysis and design.

is immune to power flow reversal in the NS line [2]–[4], [13] and leads to minimum levels of adverse interactions among the IZ POD and SMA POD controllers.

Other important practical aspects of POD design, such as the need for a variable POD gain with the level of power transfer, are not dealt with in this paper since practically all POD relevant scenarios relate to maximum transfer levels (see Table I).

The block diagrams for the power system transfer function $G_{23}(s)$ and the POD controller employed in its feedback stabilization are shown in Fig. 3 together with $G_{21}(s)$ and $G_{22}(s)$, which model two exogenous disturbances. Symbols B_{SC} and P_{SC} denote the effective susceptance and the active power deviations through the TCSC, respectively. Hence, the open-loop model under analysis, $G(s)$, is a (2×3) transfer matrix:

$$\begin{bmatrix} B_{SC} \\ P_{SC} \end{bmatrix} = \underbrace{\begin{bmatrix} 0 & 0 & 1 \\ G_{21} & G_{22} & G_{23} \end{bmatrix}}_{G(s)} \begin{bmatrix} P_{mec}^{TUC} \\ P_{mec}^{SMA} \\ B_{SC} \end{bmatrix} \tag{1}$$

where the Laplace variable s has been dropped for the sake of simplicity and $G_{11}(s) = B_{SC}(s)/P_{mec}^{TUC}(s)$ and $G_{12}(s) = B_{SC}(s)/P_{mec}^{SMA}(s)$ are the disturbance channels, whereas $G_{23}(s)$ is the control channel. The TCSC output B_{SC} (controlled output) is sensitive to disturbances in P_{mec}^{TUC} and P_{mec}^{SMA} only in closed loop, since $G_{11}(s) = G_{12}(s) = 0$ (cf. equations (1) and (2)).

The transfer function chosen for damping the NS mode is $G_{23}(s) = P_{SC}^{POD}(s)/B_{SC}(s)$, P_{SC}^{POD} being the associated active power deviations through the TCSC. The state-space realization of this transfer function has a direct transmission term ($d = 4.88 \times 10^{-3}$).

The inputs to the transfer functions $G_{21}(s)$ and $G_{22}(s)$ are the mechanical powers at the Tucuruí power plant, located at the North part of BIPS, and at the Serra da Mesa power plant, located close to the SMA TCSC. The output variables are the resulting active power deviations through the TCSC, P_{SC}^{TUC} and P_{SC}^{SMA}, respectively (refer to Fig. 2 and Fig. 3).

The total active power deviations through the TCSC (measured output) is given by: $P_{SC} = P_{SC}^{TUC} + P_{SC}^{SMA} + P_{SC}^{POD}$. The closed-loop multivariable system is then described by the following transfer matrix:

$$\begin{bmatrix} B_{SC} \\ P_{SC} \end{bmatrix} = \underbrace{\frac{1}{\Delta}\begin{bmatrix} -G_{21}POD & -G_{22}POD & 1 \\ G_{21} & G_{22} & G_{23} \end{bmatrix}}_{G_{cl}(G,POD)} \begin{bmatrix} P_{mec}^{TUC} \\ P_{mec}^{SMA} \\ B_{SC}^{ref} \end{bmatrix} \tag{2}$$

with $\Delta(s) = 1 + G_{23}(s)POD(s)$.

III. Computation of Modal Equivalents

Let $G(s) = \left[\mathbf{c}^T(sI - A)^{-1}\mathbf{b} + d\right]$ be a generic scalar transfer function, where dynamical and identity matrices A, $I \in \mathbb{R}^{n \times n}$, input and output vectors $\mathbf{b}$, $\mathbf{c} \in \mathbb{R}^n$ and the direct transmission term $d \in \mathbb{R}$. Computation of a reduced modal approximation $G_r(s)$ can be interpreted as performing a similarity transformation T on the original system $G(s)$ yielding:

$$\left[\begin{array}{c|c} T^{-1}AT & T^{-1}\mathbf{b} \\ \hline \mathbf{c}^T T & d \end{array}\right] \triangleq \left[\begin{array}{cc|c} \widehat{A}_1 & 0 & \widehat{\mathbf{b}}_1 \\ 0 & \widehat{A}_2 & \widehat{\mathbf{b}}_2 \\ \hline \widehat{\mathbf{c}}_1^T & \widehat{\mathbf{c}}_2^T & d \end{array}\right], \tag{3}$$

where $\{spec(\widehat{A}_1)\}$ and $\{spec(\widehat{A}_2)\}$ are the set of the r dominant and, respectively, the $n-r$ non-dominant modes of A, and then defining the reduced model as $G_r(s) \triangleq \widehat{\mathbf{c}}_1^T \left(sI - \widehat{A}_1\right)^{-1} \widehat{\mathbf{b}}_1 + d$. Without loss of generality, we assume $d = 0$ in the following.

Matrix A is assumed to be block-diagonal. That is, the original model is already additively decomposed, which can be easily obtained for large scale systems by using the algorithm described in [23], [24]. Equation (4) describes the state-space realization $(A, \mathbf{b}, \mathbf{c})$ of $G(s)$, where $\{spec(A_i), i = 1, ..., k\}$ contains the set of poles of $G(s)$ and $k = n_c + n_r < n$. Integers n_r and n_c are respectively the number of real and complex modes, and $n_r + 2n_c = n$. Block matrices A_i are of dimensions (1×1) or (2×2), for real or complex modes, respectively, and $\mathbf{b}_i$, $\mathbf{c}_i^T$ are vectors of compatible dimensions.

$$\left[\begin{array}{c|c} A & \mathbf{b} \\ \hline \mathbf{c}^T & d \end{array}\right] = \left[\begin{array}{ccc|c} A_1 & \dots & 0 & \mathbf{b}_1 \\ \vdots & \ddots & \vdots & \vdots \\ 0 & \dots & A_k & \mathbf{b}_k \\ \hline \mathbf{c}_1 & \dots & \mathbf{c}_k & 0 \end{array}\right] \tag{4}$$

The parallel realization (4) can be described by the partial fraction decomposition (5):

$$G(s) = \sum_{i=1}^{k} G_i(s) = \sum_{i=1}^{k} \mathbf{c}_i^T (sI - A_i)^{-1} \mathbf{b}_i, \tag{5}$$

where $G_i(s)$, $i = 1, ..., k$, are 1^{st}- or 2^{nd}-order rational functions, according to the dimensions of A_i.

Let the n eigenvalues of A and the corresponding right and left eigenvectors be given by the eigentriplets $(\lambda_i, \mathbf{x}_i, \mathbf{y}_i)$, $i = 1, ..., n$, and let the right and left eigenvectors be scaled so that $\mathbf{y}_i^* \mathbf{x}_i = 1$, where $\mathbf{y}_i^*$ denotes the Hermitian of $\mathbf{y}_i \in \mathbb{C}^n$. Note that $\mathbf{y}_i^* \mathbf{x}_j = 0$ for $i \neq j$. Then the transfer function $G(s)$ can also be expressed as a sum of residues R_i over first-order polynomials:

$$G(s) = \sum_{i=1}^{n} \frac{R_i}{s - \lambda_i}, \tag{6}$$

where $R_i = (\mathbf{c}^T \mathbf{x}_i)(\mathbf{y}_i^* \mathbf{b})$, with $\mathbf{c}^T \mathbf{x}_i$ and $\mathbf{y}_i^* \mathbf{b}$ being, respectively, the observability and the controllability factors of λ_i. It is worth mentioning that all k fractions in decomposition (5) have real coefficients while some of n fractions in (6) may have complex coefficients.

If the eigenvalues λ_i are sorted in descending order (with increasing i) of dominance, according to some chosen MDI, and the first r dominant modes are retained in the reduced-model $G_r(s)$, the error incurred in modal truncation depends on the $n - r$ omitted modes, i.e., the modes labeled $r + 1$ to n:

$$\widetilde{G}(s) \triangleq G(s) - G_r(s) = \sum_{i=r+1}^{n} G_i(s), \tag{7}$$

where $G_i(s)$, $i = r+1, ..., n$, are the $n-r$ non-dominant modal components of $G(s)$ in (5). Assuming that $G(s) \in \mathcal{L}_\infty$, i.e., $G(s)$ is bounded on the imaginary axis, one can define an upper bound on the $\mathcal{L}_\infty$ norm [25] of the error:

$$\begin{aligned} \|\widetilde{G}(s)\|_\infty \;&\triangleq\; \text{ess} \sup_{\omega \in \mathbb{R}} \{\overline{\sigma}[\widetilde{G}(j\omega)]\} = \|G(s) - G_r(s)\|_\infty \\ &= \left\| \sum_{i=r+1}^{n} G_i(s) \right\|_\infty \leq \sum_{i=r+1}^{n} \|G_i(s)\|_\infty, \end{aligned} \tag{8}$$

where $\overline{\sigma}[\widetilde{G}(j\omega)]$ is the largest singular value of $\widetilde{G}(j\omega)$ and ess $\sup[\overline{\sigma}(\omega)]$ is the essential supremum of $\overline{\sigma}(\omega)$ [25].

Although there are different MDIs [19]–[21], this paper utilizes the MDI defined in [26] as the $\mathcal{L}_\infty$-norm of each modal component $G_i(s)$ in (5) (contrarily to [21], for example, which considers the infinite norm of each component in (6)), which naturally results in minimum upper bounds on the error (8) while preserving the dominant poles and associated residues defined in (6). This MDI is referred here as $\mathcal{L}_\infty-$MDI and showed a slightly better performance than the MDI recommended in [21], which requires 220 states to produce Bode plot approximations of equivalent accuracy (see Fig. 4−6). These definitions also apply to a MIMO $G(s)$ in (1) since $G_i(s)$ in (5) can be defined as MIMO transfer functions and R_i in (6) as residue matrices.

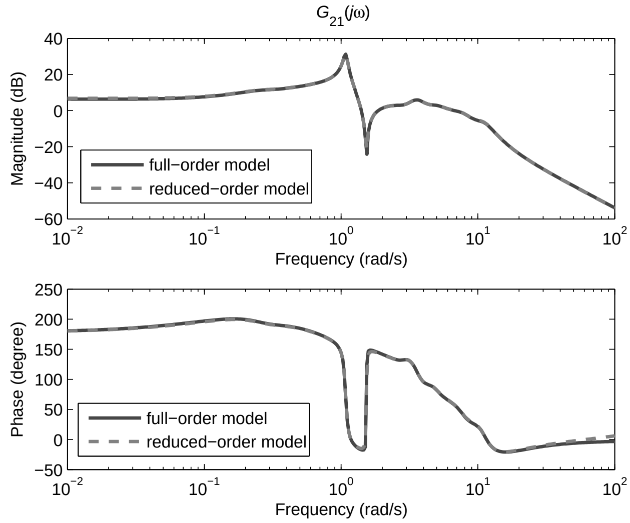

Fig. 4. Bode plots for $G_{21}(s)$ considering the full BIPS model (1,664 states) and the reduced 200-state model (Scenario I).

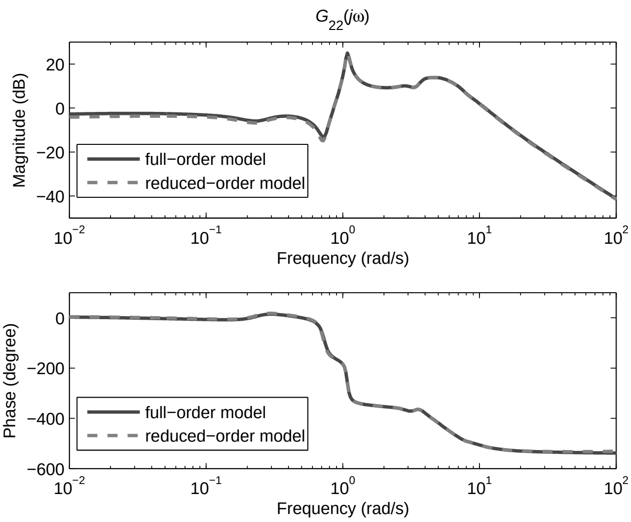

Fig. 5. Bode plots for $G_{22}(s)$ considering the full BIPS model (1,664 states) and the reduced 200-state model (Scenario I).

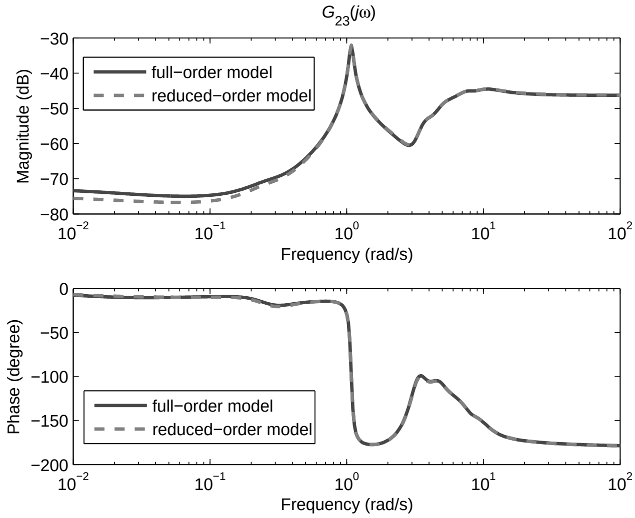

Fig. 6. Bode plots for $G_{23}(s)$ considering the full BIPS model (1,664 states) and the reduced 200-state model (Scenario I).

IV. NONSMOOTH TIME-DOMAIN DESIGN METHOD

Large scale power system oscillation damping control is a typical example of how realistic design problems frequently impose structure constraints on the controller. This is indeed the situation here inasmuch as a full-order controller design is not a feasible solution from an implementation as well as a computational point of view and reduced controller order becomes mandatory. The classical approach in the robust control literature to deal with reduced-order constraints consists in combining a full-order synthesis technique with some model reduction scheme (see [27], for instance). In this case, either the plant is reduced a priori to the maximal acceptable controller order, or the synthesized full-order controller is reduced a posteriori. Unfortunately, these approaches are in general prone to failure whenever the difference between model and controller orders is sizable, as happens here.

The NonSmooth Time-Domain (NSTD) controller design technique presented in [16], [17] has the capability to handle a vast array of controller structures and architectures, including reduced-order, so it may dispense with the above reduction schemes. Another interesting feature is that it avoids Lyapunov variables, whose space dimension grows quadratically with the system order and represents a major impediment to the practical use of approaches based on linear or bilinear matrix inequalities. Consequently, it is better suited to high-order power systems applications.

The correlation between the transient and frequency responses is indirect, except for the simple case of second-order systems. Robust controller design methods that may directly impose time-domain constraints are therefore highly attractive. The NSTD technique can naturally handle such constraints since it is based on the time-domain shaping of closed-loop system responses to fixed inputs. More specifically, the design objective is to find a stabilizing controller such that the closed-loop response $z(t)$ to a given test input $w(t)$ satisfies the envelope constraints

$$l_z(t) \leq z(t) \leq u_z(t),\ \forall t \geq 0, \tag{9}$$

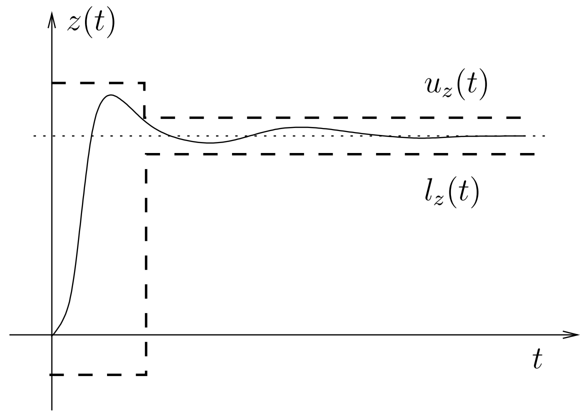

Fig. 7. Shape-constraints on the step response

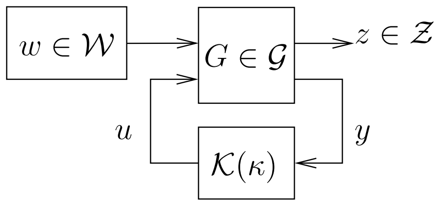

Fig. 8. General framework for the nonsmooth time-domain design

where l_z and u_z are lower and upper bounds on the closed-loop responses, as illustrated in Fig. 7.

The general framework of the NSTD design technique is represented by the standard form description ($u \in \mathbb{R}^{m_2}$ and $y \in \mathbb{R}^{p_2}$) indicated in Fig. 8, where the multivalued plant $G(s)$ is considered to take values in a finite family of linear plants $\mathcal{G} := \{G^1, \ldots, G^p\}$. Each plant G in the family $\mathcal{G}$ in feedback loop with a single controller $K(s)$ is subject to one or several input signals w selected in a finite signal generator set $\mathcal{W} := \{w^1, \ldots, w^d\}$. Those signals are in general deterministic test inputs such as steps, ramps, sinusoids, etc. The closed-loop response of $G \in \mathcal{G}$ to a signal $w \in \mathcal{W}$ gives rise to a finite family of closed-loop responses $z \in \mathcal{Z}$, where $\mathcal{Z} := \{z^1, \ldots, z^r\}$. The synthesis procedure consists in the search of a fixed-structure controller $K(s)$ such that appropriate time-domain specifications in (9) are achieved for all instances $z \in \mathcal{Z}$.

The POD design problem considered here is among the various practical situations that can be handled by the above set-up: the original system is described by multiple operating conditions, each constituting a linear plant in the family $\mathcal{G}$ that will be tested against inputs $w \in \mathcal{W}$ on the exogenous disturbance channels.

In order to deal with different controller structures, it is convenient to introduce the controller parametrization in state-space

$$\mathcal{K}(\kappa) := \begin{bmatrix} A_K(\kappa) & B_K(\kappa) \\ C_K(\kappa) & D_K(\kappa) \end{bmatrix}, \tag{10}$$

where κ designates the design variables, and the mapping $\mathcal{K}:\ \mathbb{R}^q \to \mathbb{R}^{(m_2+k)\times(p_2+k)}$ is considered to be continuously differentiable but otherwise arbitrary. As a result, other structures of interest as PID, decentralized, static controller, etc. are easily captured.

Amplitude and rate constraints can be formulated for the control signals. Amplitude constraints can be used to keep signals at levels where they do not saturate, thus preserving linearity in controller response, as much as possible.

In practical applications, it is useful to distinguish between hard and soft constraints in (9). Consider a partition of $J := \{1, \ldots, r\}$, indexing $\mathcal{Z}$, into disjoint subsets S and H, i.e., $J = S \cup H$, $S \cap H = \emptyset$, where S should be seen as the index set for soft constraints and H the one for hard constraints. The set $\mathcal{Z}$ of closed-loop responses is partitioned correspondingly in the form $\mathcal{Z} = \mathcal{Z}_S \cup \mathcal{Z}_H$. Noting that the envelope constraints in (9) can be alternatively described by

$$f_z(\kappa) := \max_{t \geq 0} \{[z(\kappa,t) - u_z(t)]_+,\ [l_z(t) - z(\kappa,t)]_+\} \leq 0,$$

where $[g]_+ := \max\{g, 0\}$, the notion of hard and soft constraints becomes clear through the following program translating the overall design problem:

$$\begin{array}{ll} \underset{\kappa \in \mathbb{R}^q}{\text{minimize}} & \max_{z \in \mathcal{Z}_S} f_z(\kappa) \\ \text{subject to} & \max_{z \in \mathcal{Z}_H} f_z(\kappa) \leq 0. \end{array} \tag{11}$$

A solution to program (11) necessarily meets the constraints $z \in \mathcal{Z}_H$ while constraints related to $z \in \mathcal{Z}_S$ will be achieved only when the objective function falls below 0.

Program (11) is a difficult mathematical programming problem due to its nonconvex and nonsmooth nature. A specialized nonsmooth optimization technique developed in [16], [28], [29] is used here to obtain, in a single run, a POD design (POD_3) that is of the same order but more robust than the two POD conventional designs (POD_1 and POD_2).

V. Conventional POD Controllers

A major problem in the POD design of the SMA TCSC lies in the potential risk of equipment hitting limits following exogenous disturbances, as described in Section II.

The original SMA POD controller (POD_1) is derived from the modulus of the line active power that is phase-lagged by 90 degrees at the frequency of the NS mode [1]–[4]:

$$\begin{aligned} POD_1(s) &= KF_1(s)F_2(s), \\ K &= -1370, \\ F_2(s) &= \left(\frac{1}{0.8s+1}\right)^2 \left(\frac{0.3s+1}{2.2s+1}\right)^2, \\ F_1(s) &= \left(\frac{0.8s}{0.02s+1}\right)\left(\frac{2.5s}{2.5s+1}\right). \end{aligned} \tag{12}$$

The phase-lag solution (POD_1), currently implemented in the SMA POD, does not intrinsically attenuate dynamic activity in the low-frequency range (Fig. 9), and the high-gain closed-loop instability emerges through a low-frequency mode, as will be shown in Fig. 14.

The alternative phase-lead solution (POD_2) is described in [30] and comprises a gain K, a washout $W(s)$, a derivative block in association with a 3^{rd}-order Butterworth ($B(s)$) and a notch filter $N(s)$:

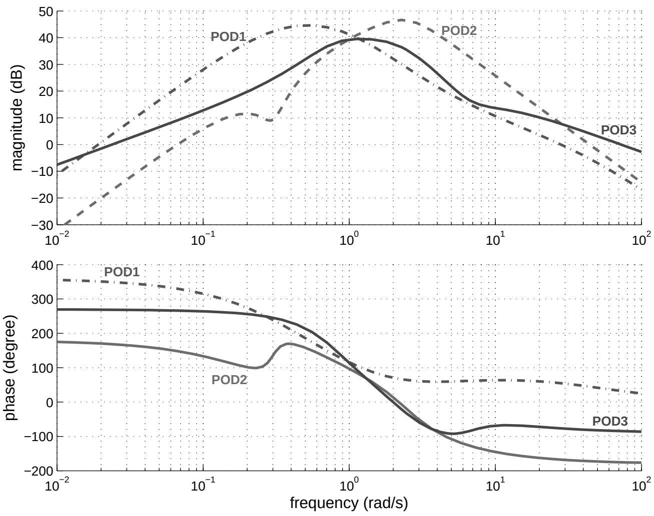

Fig. 9. Bode plots for the phase-lag (POD_1, dash-dot), phase-lead (POD_2, dashed) and nonsmooth (POD_3, solid) PODs.

$$\begin{aligned} POD_2(s) &= KW(s)B(s)N(s), \\ K &= 125, \\ W(s) &= \left(\frac{2s}{2s+1}\right), \\ B(s) &= \left(\frac{15.63s}{s^3+5s^2+12.5s+15.63}\right), \\ N(s) &= \left(\frac{s^2+0.09s+0.09}{s^2+0.6s+0.09}\right). \end{aligned} \tag{13}$$

The notch filter, $N(s)$, with a damping ratio $\zeta = 0.15$, heavily attenuates modal components around $\omega_z = 0.3$ rad/s while having reduced impact on the NS mode frequency (1.1 rad/s).

The phase-lead solution (POD_2) increases dynamic activity in a high-frequency range with the high-gain closed-loop instability emerging through a higher frequency mode (5 rad/s), as will also be shown in Fig. 14.

VI. Results

Time and frequency simulation results for POD_1 and POD_2 solutions are repeated in this paper, but only to allow comparing their dynamic performances with that of the proposed POD_3 design by the NSTD method.

A. POD Synthesis by NSTD Method for 4 Scenarios

Two structural constraints are imposed on the POD: reduced order and washout filtering. The controller structure is chosen accordingly as

$$POD_3(s) = \frac{s}{s+p}\,\widehat{K}(s), \tag{14}$$

where $\widehat{K}(s)$ is a 5th-order strictly proper transfer function, and the position of the real washout pole $-p$ is also a decision variable of the optimization program.

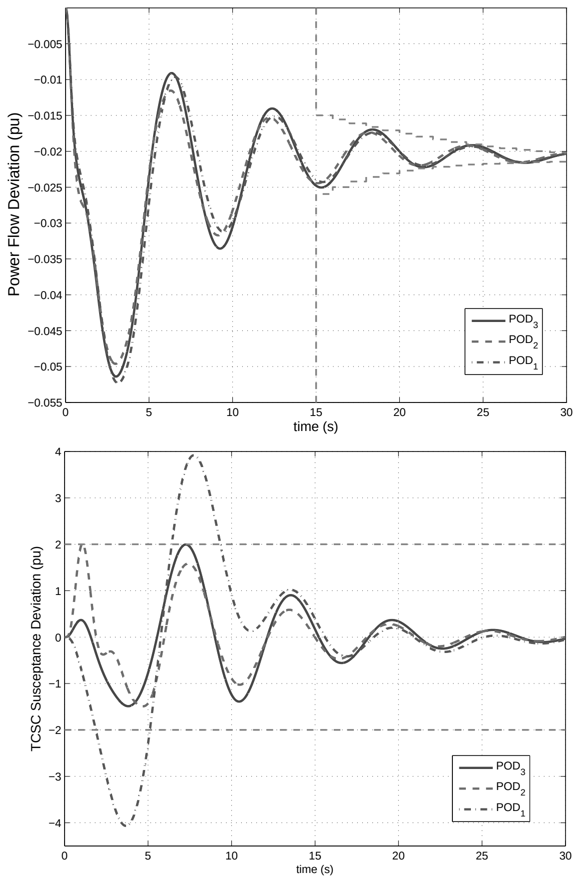

Fig. 10. Linear simulations for disturbance at Tucuruí (Scenario I).

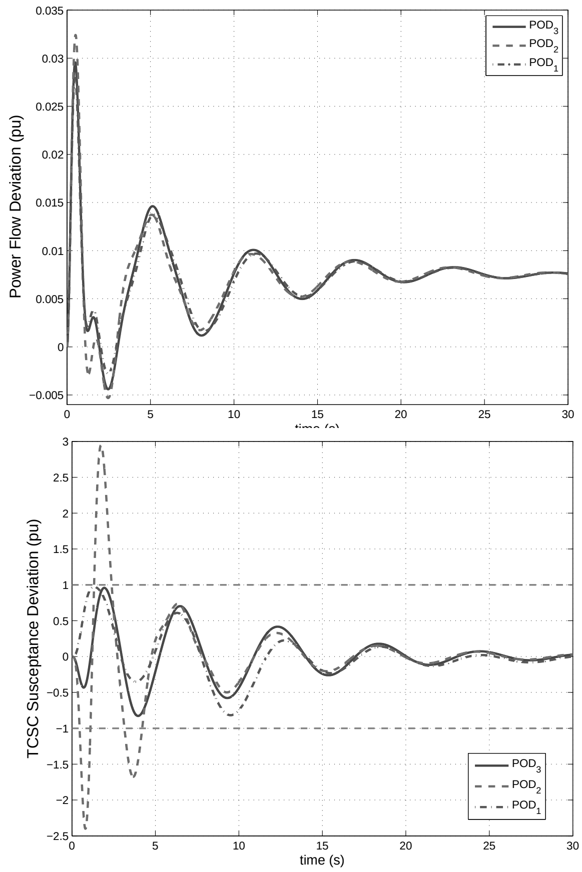

Fig. 11. Linear simulations for disturbance at Serra da Mesa (Scenario I).

Note that controller order is a user-defined parameter and is not affected by the order of the models in $\mathcal{G}$, that may be selected as desired and may even differ from one another. Unfortunately, there is normally a trade-off between reduced computational effort and satisfactory system dynamics description. Similar comments apply to the number of scenarios considered for synthesis.

Four representative power flow scenarios are chosen for synthesis: scenarios C, D, I and Q in Table I. The associated synthesis models $G(s)$ in (1) are selected as 200th-order transfer function modal equivalents obtained with the use of $\mathcal{L}_\infty-$MDI (section III). These reduced models adequately describe the system dynamics (see Bode plots in Figs. $4-6$) while permitting a considerable reduction in the computation time of the NSTD method.

Test signals are selected as steps, which are applied to the exogenous disturbances. More precisely, each instance $w \in \mathcal{W}$ corresponds to a step being applied to one of the disturbances while the other one is kept to zero.

The time envelope constraints that have been defined for the line power flow deviation P_{SC} and for the TCSC susceptance deviation B_{SC} are depicted in Fig. 10 and 11.

Maximum amplitude constraints for the linear response of B_{SC} were defined in such a way that the susceptance transient peaks produced by POD_3 are smaller than, or at least equivalent to, the largest linear transient peaks produced by POD_1 or POD_2 for test signals applied to both disturbance channels. Since reducing large transient peaks following exogenous disturbances represents a priority, B_{SC} linear transient peak values are defined as hard constraints in program (11).

The required NS mode damping is achieved by shaping the power flow deviation response P_{SC}. Its transient is forced to lie inside an exponentially decaying envelope, as depicted in Fig. 10. Note that this envelope was drawn with focus on the lowest frequency oscillatory component at the tail end of the oscillation. The design procedure can take such characteristics of the plant into account thus avoiding unrealistic solutions. The decay rate of the exponential envelopes are determined to provide 15% damping at the corresponding open-loop NS mode frequencies. Power oscillation damping ratios are defined as soft constraints in program (11).

Susceptance deviation (B_{SC}) levels are imposed through tests in both disturbance channels. On the other hand, one single power flow deviation response per scenario is enough to ensure the required NS mode damping so P_{SC} constraints have been considered solely for the case of Tucuruí disturbances.

The NSTD design algorithm solves program (11) in 199 iterations, requiring 106 minutes CPU time on a 2.8GHz Pentium D processor with 1GB RAM. The POD controller parameters in (14) have been obtained as $p = 1.4382$ and

$$\widehat{K}(s) = \frac{73.21s^4 + 381.9s^3 + 3001s^2 - 2391s - 1409}{s^5 + 10.75s^4 + 33.45s^3 + 62.68s^2 + 46.42s + 23.39}.$$

TABLE I
BIPS POWER FLOW SCENARIOS AND ASSOCIATED NS MODE [18]

Scenario identification	**Scenario Description**				**NS mode**	
	System Load (GW)	Generation at Tucuruí (MW)	NS Power flow (MW)	Flow direction	ω_d (Hz)	ζ (%)
A- L00GMAXE	30.9	3355	0	———	0.24	15.03
B- L00GMINE	30.8	1300	7	N → S	0.23	7.64
C- LNSGMAXE	31.0	3520	968	N → S	0.24	10.05
D- LNSGMINE	31.0	2280	962	N → S	0.21	5.69
E- LSNGMAXE	30.9	2352	1015	S → N	0.24	15.75
F- LSNGMINE	30.8	1300	1029	S → N	0.25	12.80
G- M00GMAXE	47.4	3520	4	N → S	0.22	12.99
H- M00GMINE	47.4	1626	3	N → S	0.19	4.47
I- MNSGMINE	47.6	2684	974	N → S	0.17	3.11
J- MSNGMAXE	47.4	2508	1032	S → N	0.21	12.55
K- MSNGMINE	47.4	1300	1043	S → N	0.21	9.27
L- P00GMAXE	52.9	3267	3	N → S	0.21	13.50
M- P00GMINE	52.8	2674	5	N → S	0.20	11.27
N- PNS1000E	52.7	3520	966	N → S	0.19	8.62
0- PNSGUNIE	52.9	3520	703	N → S	0.20	10.74
P- PSNGMAXE	52.9	2265	1041	S → N	0.20	12.50
Q- PSNGMINE	52.9	1764	1033	S → N	0.20	11.06

B. Synthesis by NSTD Method with Additional Scenarios

As will be seen below, the POD_3 controller performs well for all scenarios, although only 4 scenarios have been considered during the synthesis. Unfortunately, this is not always true, and the final closed-loop system performance may turn out to be unsatisfactory for scenarios that have not been dealt with. In that case, a natural alternative is to perform a new design with an enriched synthesis models family $\mathcal{G}$ that also takes those previously missing critical scenarios into account.

In order to examine whether the consequent increase in the computational effort would render the design problem intractable, a series of POD syntheses have been performed where additional scenarios were progressively incorporated. Table II relates the number of scenarios taken into consideration to the resulting average computation time in minutes per iteration. The 4 scenarios case represents the basic minimum POD_3 design, the 5 scenarios case consists in envelope time constraints relative to another scenario being added to the specifications of the previous case, and so forth. Note that the running time per iteration increases linearly with the number of scenarios and that the NSTD method is computationally efficient even when all scenarios are considered. This is a remarkable result owing to the fact that 2 test signals are applied for each one the 11 scenarios. This means that each function evaluation in program (11) comprises 22 time-domain simulations involving 200th-order models. Actually, the execution time could still be improved since these simulations are independent from one another and thus may be performed simultaneously in a parallel computer implementation.

TABLE II
EVOLUTION OF THE SYNTHESIS COMPUTATIONAL EFFORT

# of scenarios	average min/iter	# of scenarios	average min/iter
4	0.54	8	1.59
5	0.72	9	1.81
6	0.86	10	2.00
7	1.42	11	2.21

C. Linear Analysis for Multiple Scenarios

Seventeen power flow scenarios, identified by single capital letters and listed in Table I, were analyzed in [18], but only 11 scenarios having relevant NS power transfers are considered here. Fig. 12 displays the locations in the complex plane of the poles (eigenvalues) associated with the NS mode for the various scenarios. These poles may be efficiently computed when using selective eigenanalysis [23], [24]. Similarly to the POD original design POD_1, both phase-lead POD_2 and nonsmooth POD_3 solutions show robust stabilization. Note that the POD controllers are disconnected when the line active power flow is smaller than 200 MW (Scenarios A, B, G, H, L, M), for it is a known fact that TCSC controllability is much reduced for small line loadings and becomes identical to zero for zero flow conditions. It is worth mentioning that the alternative PSS-based damping solution, reported in [9], [18] and involving changes in the PSS structure of three large Northeast power plants, does not turn ineffective for reduced NS power transfer levels and was actually commissioned as a complementary damping source since late 2005.

The Bode plots for the phase-lag (POD_1), phase-lead (POD_2) and NSTD (POD_3) designs for the POD controller are compared in Fig. 9. Note that the three PODs are 6th-order controllers. These three controllers have about the same gain and phase at the frequency of the NS mode (1.1 rad/s) but show quite different levels of activity in the low- and high-frequency ranges, as expected. The parameter values for POD_1 and POD_2 were given in Section VI-A.

Bode magnitude plots of the two closed-loop disturbance channels, in Scenario I, when employing $POD_1(s)$, $POD_2(s)$ or $POD_3(s)$ controllers are pictured in Fig. 13. Note that the zero of the notch filter is visible in the Bode plot of the closed-loop disturbance channel (Fig. 13) for $POD_2(s)$, a fact that is readily understood from the analysis of Eq. (2). More importantly, $POD_3(s)$ controller is the only one to show reduced dynamic activity in both lower and higher frequency ranges, anticipating better transient performances for the two disturbance channels. The time response plots in Fig. 10 are for a mechanical power step disturbance at the Tucuruí (TUC)

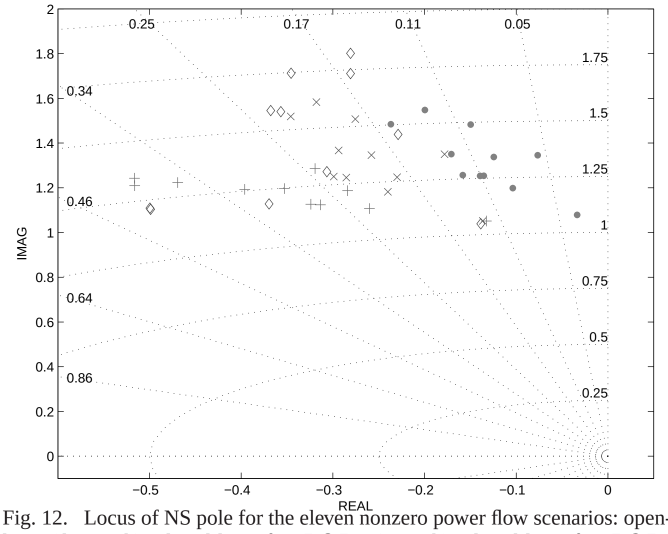

Fig. 12. Locus of NS pole for the eleven nonzero power flow scenarios: open-loop (dot-mark), closed-loop for POD_1 (x-mark), closed-loop for POD_2 (plus-mark) and closed-loop for POD_3 (diamond-mark).

generating plant, in scenario I. The results indicate that both POD_2 and POD_3 have adequate performances, while POD_1 shows large transients in B_{SC}.

Fig. 14 shows the critical root-locus branches, in scenario I, for each POD controller, as the gains for the 3 PODs are raised. All POD controllers are seen to cause system oscillatory instability for high values of gain. They have, however, a comfortably large gain range for which the system is adequately stabilized (except for POD_2, which has a smaller gain margin). High gain instabilities for POD_1, POD_2, and POD_3 designs appear in the form of sustained oscillations at 0.45 rad/s, 3.7 rad/s and 1.8 rad/s, respectively, as seen in Fig. 14.

The time response plots in Fig. 11 are for a mechanical power step disturbance at the Serra da Mesa (SMA) generating plant for the same scenario. Note that, in this case, both POD_1 and POD_3 have adequate performances, while POD_2 shows large transients in B_{SC}.

Fig. 15 and Fig. 16 show the NS line power (P_{SC}) transients and the TCSC effective susceptance (B_{SC}) transients, induced by step disturbances P_{mec}^{TUC}, applied at 3s, and P_{mec}^{SMA}, applied at 40s. Variables P_{SC}, B_{SC}, P_{mec}^{TUC}, P_{mec}^{SMA} are depicted in Fig. 2. Fig. 15 shows the 3 POD controllers confer approximately the same damping to the NS mode (results relate to Scenario I). Fig. 16 shows the B_{SC} transients for POD_1 and POD_2 are larger than those of POD_3, confirming the more robust dynamic performance of the latter.

Similar simulations were carried out for all scenarios, and the peaks for the B_{SC} transients determined for the two disturbances. The obtained results are summarized in the bar-charts of Fig. 17, confirming the superior performance of POD_3 in all 11 scenarios.

VII. Concluding Remarks

Critical power system controllers, like the PODs in the North-South Brazilian Interconnection for the year 1999 configuration, deserve special attention and the use of sophisticated design methods. The authors attempted designing PODs

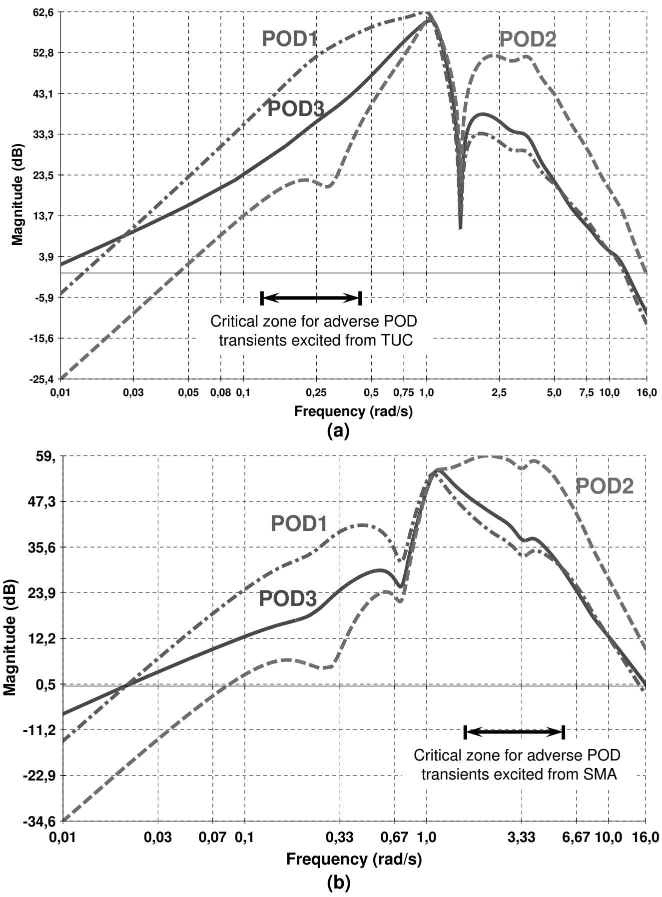

Fig. 13. Bode magnitude plots of the closed-loop disturbance channel for Scenario I: POD_1, dash-dot; POD_2, dashed; and POD_3, solid; (a) $B_{SC}(j\omega)/P_{mec}^{TUC}(j\omega)$; (b) $B_{SC}(j\omega)/P_{mec}^{SMA}(j\omega)$.

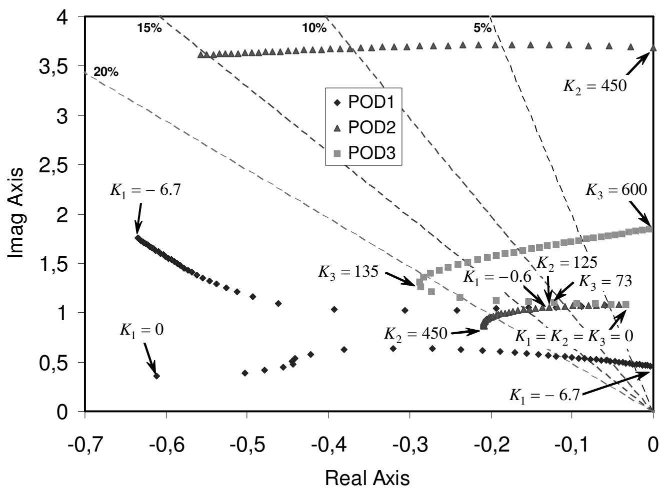

Fig. 14. Critical root-locus branches for the 3 PODs (Scenario I).

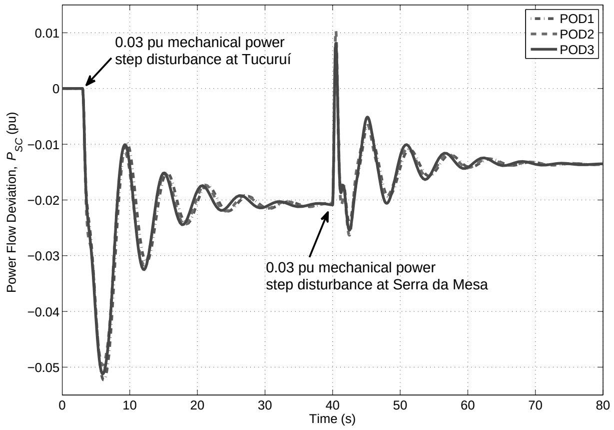

Fig. 15. Line power transients (P_{SC}) following step disturbances P_{mec}^{TUC} (at 3s) and P_{mec}^{SMA} (at 40s) for Scenario I, refer to Fig. 2.

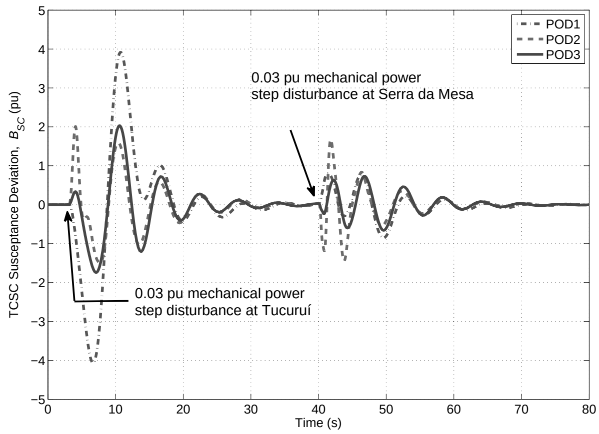

Fig. 16. Transients in B_{SC}, the TCSC effective susceptance, following step disturbances P_{mec}^{TUC} (at 3s) and P_{mec}^{SMA} (at 40s) for Scenario I, refer to Fig. 2.

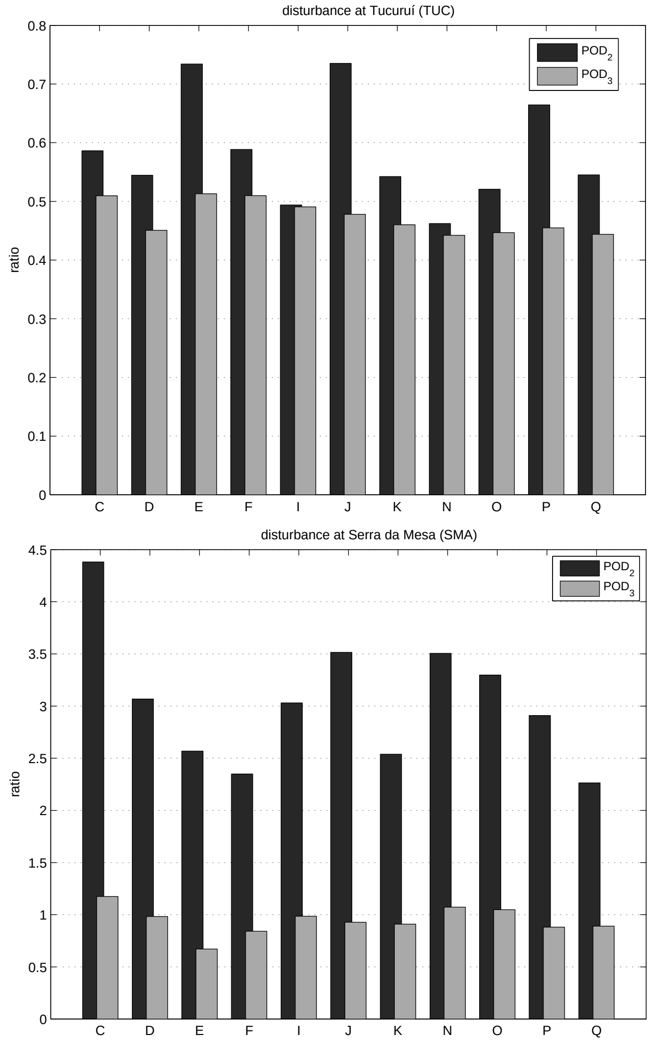

Fig. 17. Ratios between B_{SC} transient peaks ($POD_{2,3}/POD_1$) following an applied step in the disturbance channels.

derived from other signals, local or remote. The difference between North and South average angles (remote measurements), as an alternative POD signal, produced very similar results to the local-based line power signal (P_{sc}), the latter being therefore rated the best in these studies, as well as in practice and also used throughout this paper. The use of local signals such as bus frequency led to higher adverse interaction with other modes, which could also become critical.

The nonsmooth time-domain design method proposed in this paper reveals to be a valuable addition to the power system dynamics and control engineer's toolkit. Multiple scenarios specifications are easily incorporated in the synthesis procedure as well as the specific structure of POD controllers. Extensive numerical experiments on simultaneous design of up to 11 scenarios involving 200th-order models suggest that the nonsmooth approach is a practical and efficient technique in challenging applications such as the one discussed in this paper.

ACKNOWLEDGMENTS

The authors would like to thank CEPEL and ELETROBRAS for providing the Brazilian interconnected power system model, and Nilo José Pereira de Macedo (FURNAS) and Guilherme Sarcinelli Luz (FURNAS) for their valuable suggestions.

REFERENCES

[1] N. Martins, H. J. C. P. Pinto, C. Gama, J. A. Cavalcanti, R. L. Leoni, R. V. Souto, N. J. P. Nilo, and M. J. X. Eiras, "Oscillation damping analysis and control studies of the future interconnection between the North-Northeast and South-Southeast systems," in *Proc. V Symposium of Specialists in Electric Operational and Expansion Planning - SEPOPE*, Recife, Brazil, 1996.

[2] C. Gama, R. L. Leoni, J. C. Salomão, J. B. Gribel, R. Fraga, M. J. X. Eiras, W. Ping, A. Ricardo, and J. Cavalcanti, "Brazilian North-South interconnection - application of thyristor controlled series compensation to damp inter-area oscillation mode," in *Proc. Symposium of Specialists in Electric Operational and Expansion Planning - SEPOPE*, Brazil, 1998.

[3] C. Gama, L. Ängquist, G. Ingeström, and M. Noroozian, "Commissioning and operative experience of TCSC for damping power oscillation in the Brazilian north-south interconnection," in *Proc. CIGRE Session 2000*, Paper 14-104, Paris, France, 2000.

[4] G. S. Luz, N. J. P. Macedo, and V. R. Oliveira, "Furnas TCSC - an example of using different simulation tools for performance analysis," in *Proc. International Conference on Power System Transients*, Rio de Janeiro, Brazil, 2001.

[5] N. Chistl, R. Hedin, K. Sadek, P. Lutzelherger, P. E. Krause, S. M. McKenna, A. H. Monloya, and D. Torgerson, "Advanced series compensation with thyristor controlled impedance," *CIGRE paper 14/37/38-05*, 1992.

[6] A. J. F. Keri, B. J. Ware, R. A. Byron, M. Chamia, P. Halvarsson, and L. Ängquist, "Improving transmission system performance using controlled series capacitors," *CIGRE paper 14/37/38-07*, 1992.

[7] R. J. Piwko, C. A. Wegner, D. B. L, B. C. Furumasu, and J. D. Eden, "The Slatt thyristor controlled series capacitor project-design, installation, commissioning, and system testing," *CIGRE paper 14-104*, 1994.

[8] IEEE FACTS Working Group 15.05.15 in cooperation with CIGRE, *FACTS Overview*. IEEE Special Publication 96-TP-108, 1996.

[9] N. Martins, A. A. Barbosa, J. C. R. Ferraz, M. G. Santos, A. L. B. Bergamo, C. S. Yung, V. R. Oliveira, and N. J. P. Macedo, "Retuning stabilizers for the north-south Brazilian interconnection," in *Proc. IEEE Power Engineering Society Summer Meeting*, vol. 1, Edmonton, Alberta, Canada, Jul 1999, pp. 58–67.

[10] CIGRE TF 38.02.16, "Impact of the interactions among power system controls," CIGRE, Paris, Tech. Rep. 166, Jul 2000.

[11] L. Angquist, B. Lundin, and J. Samuelsson, "Power oscillation damping using controlled reactive power compensation - a comparison between series and shunt approaches," *IEEE Trans. Power Syst.*, vol. 8, no. 2, pp. 687–700, May 1993.

[12] M. Noroosian and G. Andersson, "Damping of power system oscillations by use of controllable components," *IEEE Trans. Power Delivery*, vol. 9, no. 4, pp. 2046–2054, Oct 1994.

[13] E. V. Larsen, J. J. Sanchez-Gasca, and J. H. Chow, "Concepts for design of FACTS controllers to damp power swings," *IEEE Trans. Power Syst.*, vol. 10, no. 2, pp. 948–956, May 1995.

[14] G. N. Taranto and J. H. Chow, "A robust frequency domain optimization technique for tuning series compensation damping controllers," *IEEE Trans. Power Syst.*, vol. 10, no. 3, pp. 1219–1225, Aug 1995.

[15] J. J. Sanchez-Gasca and J. H. Chow, "Power system reduction to simplify the design of damping controllers for interarea oscillations," *IEEE Trans. Power Syst.*, vol. 11, no. 3, pp. 1342–1349, Aug 1996.

[16] A. M. Simões, P. Apkarian, and D. Noll, "Multi-scenario time-domain control design using a nonsmooth approach," to appear in SICPRO'09, Moscow, January 2009, http://www.cert.fr/dcsd/cdin/apkarian/t739/SICPROmultiscenario.pdf.

[17] V. Bompart, P. Apkarian, and D. Noll, "Control design in the time- and frequency-domain using nonsmooth techniques," *Syst. and Control Letters*, vol. 57, no. 3, pp. 271–282, 2008.

[18] ELETROBRAS GCOI/SCEL Task Force FT-NSPRE/R, "FT-NSPRE/R final report - Retuning stabilizers for the north-south brazilian interconnection," Rio de Janeiro, Brazil, Tech. Rep., 1998 (in Portuguese).

[19] L. A. Aguirre, "Quantitative measure of modal dominance for continuous systems," *Procedings of the 32nd Conference on Decision and Control*, pp. 2405–2410, December 1993.

[20] N. Martins, F. G. Silva, P. C. Pellanda, A. Castro, and P. E. M. Quintão, "Utilizing transfer function modal equivalents of low-order for the design of power oscillation damping controllers in large power systems," in *Proc. of the IEEE/PES General Meeting*, San Francisco, California, USA, Jun 2005, pp. 1720–1726.

[21] M. Green and D. J. N. Limebeer, *Linear Robust Control*. Englewood Cliffs, New Jersey: Prentice Hall, 1995.

[22] S. Gomes Jr., N. Martins, and C. M. J. Portela, "Computing small-signal stability boundaries for large-scale power systems," *IEEE Trans. Power Syst.*, vol. 18, pp. 747–752, May 2003.

[23] J. Rommes and N. Martins, "Efficient computation of transfer function dominant poles using subspace acceleration," *IEEE Trans. Power Syst.*, vol. 21, no. 3, pp. 1218–1226, Aug 2006.

[24] ——, "Efficient computation of multivariable transfer function dominant poles using subspace acceleration," *IEEE Trans. Power Syst.*, vol. 21, no. 4, pp. 1471–1483, Nov 2006.

[25] K. Zhou, *Essentials of Robust Control*. Upper Saddle River, NJ: Prentice-Hall, Inc., 1998.

[26] F. G. Silva, "Modal equivalents of large scale power system models for oscillation damping controller design," Master's thesis, Military Institute of Engineering, Rio de Janeiro, Brazil, 2005 (in Portuguese).

[27] G. E. Boukarim, S. Wang, J. H. Chow, G. N. Taranto, and N. Martins, "A comparison of classical, robust, and decentralized control designs for multiple power system stabilizers," *IEEE Trans. Power Syst.*, vol. 15, no. 4, pp. 1287–1292, Nov 2000.

[28] P. Apkarian, D. Noll, and A. Rondepierre, "Mixed H_2/H_∞ control via nonsmooth optimization," *SIAM J. on Control and Optimization*, vol. 47, no. 3, pp. 1516–1546, 2008.

[29] P. Apkarian and D. Noll, "Nonsmooth H_∞ synthesis," *IEEE Trans. Aut. Control*, vol. 51, no. 1, pp. 71–86, 2006.

[30] D. C. Savelli, P. C. Pellanda, N. Martins, N. J. P. Macedo, A. A. Barbosa, and G. S. Luz, "Robust signals for the TCSC oscillation damping controllers of the Brazilian north-south interconnection considering multiple power flow scenarios and external disturbances," in *Proc. of the IEEE/PES General Meeting. Presented at the Panel Session on Advanced Applications of Stability Controls*, Tampa, FL, USA, june 2007.

Alberto Mota Simões received the B.Sc. and M.Sc. degrees in electrical engineering from the Military Institute of Engineering (IME), Rio de Janeiro, Brazil, in 1998 and 2004, respectively.

He is working towards a Ph.D. degree in control engineering at the Institut Supérieur de l'Aéronautique et de l'Espace (ISAE), Toulouse, France. He has been with ONERA-CERT since 2006.

Diego Chaves Savelli received the B.Sc. and M.Sc. degrees in electrical engineering from Military Institute of Engineering (IME), Rio de Janeiro, Brazil, in 2004 and 2007, respectively.

Currently, he is a Development Engineer at Transpetro.

Paulo César Pellanda (M'05) received the B.Sc. degree from the Federal University of Technology-Paraná (UTFPR), Curitiba, Brazil, in 1985, the M.Sc. degree from Military Institute of Engineering (IME), Rio de Janeiro, Brazil, in 1993, both in electrical engineering, and the Ph.D. degree in automatic control from École Nationale Supérieure de l'Aéronautique et de l'Espace (ENSAE), Toulouse, France, in 2001.

He joined the Electrical Engineering Department of IME in 1994, where he is currently an Associate Professor. His research interests include control system applications.

Nelson Martins (SM'91−F'98) received the B.Sc. degree in electrical engineering from the University of Brasilia, Brasilia, Brazil, in 1972 and the M.Sc. and Ph.D. degrees from the University of Manchester Institute of Science and Technology, Manchester, U.K., in 1974 and 1978, respectively.

He works at CEPEL, Rio de Janeiro, Brazil, since 1978 in the development of computer tools for power system dynamics and control.

Pierre Apkarian (A'94−M'00) received the Ph.D degree in control engineering from the École Nationale Supérieure de l'Aéronautique et de l'Espace (ENSAE) in 1988 and Habilitation (HDR) in 1997. He was qualified as a professor from the Université Paul Sabatier in both automatic control and applied mathematics in 1999 and 2001, respectively.

Since 1988, he is a research scientist at ONERA-Toulouse and an associate Professor in the Maths department of Université Paul Sabatier in Toulouse. His research interests include robust and gain-scheduling control theory, LMI and nonsmooth optimization techniques with applications in aeronautics. Pierre Apkarian has served as an associate editor for the IEEE Transactions on Automatic Control.